IOP Publishing Journal of Physics G: Nuclear and Particle Physics
J. Phys. G: Nucl. Part. Phys. **47** (2020) 025105 (16pp) https://doi.org/10.1088/1361-6471/ab5325

Charge form factors of exotic nuclei in deformed Hartree–Fock–Bogolyubov calculations

Lei Wang[1], Jian Liu[1,2], Tongqi Liang[3], Zhongzhou Ren[3], Chang Xu[4] and Shuo Wang[5]

[1] College of Science, China University of Petroleum (East China), Qingdao 266580, People's Republic of China
[2] PCIF Key Laboratory of Oil and Gas Terahertz Spectroscopy and Photoelectric Detection, China University of Petroleum (East China), Qingdao 266580, People's Republic of China
[3] School of Physics Science and Engineering, Tongji University, Shanghai 200092, People's Republic of China
[4] Department of Physics, Nanjing University, Nanjing 210093, People's Republic of China
[5] Shandong Provincial Key Laboratory of Optical Astronomy and Solar-Terrestrial Environment, Institute of Space Science, Shandong University, Weihai 264209, People's Republic of China

E-mail: liujian@upc.edu.cn

Received 29 July 2019, revised 20 October 2019
Accepted for publication 31 October 2019
Published 9 January 2020

Abstract

With the development of electron scattering experiments off exotic nuclei, many theoretical researches have been devoted to investigate the nuclear charge form factors $|F_C(q)|^2$ recently. In this paper, we extend the studies of electron scattering by combing the deformed Hartree–Fock–Bogolyubov (HFB) model and the distorted wave Born approximation (DWBA) method. Comparing the theoretical $|F_C(q)|^2$ with the experimental data, the validity of the deformed HFB model to describe the nuclear density distributions can be verified for both the spherical and deformed nuclei. By further investigating the $|F_C(q)|^2$ of the isotopic chain, the effects of the nuclear deformation on the changing trends of $|F_C(q)|^2$ of isotopes are provided. For even–even Xe isotopes, the nuclear deformation can influence the positions of the diffraction minima of $|F_C(q)|^2$. For odd-A Cs isotopes, the nuclear deformation can affect the values of diffraction minima of $|F_C(q)|^2$. The studies in this paper can offer useful guidances for the coming electron scattering experiments on unstable nuclei.

Keywords: charge form factors of exotic nuclei, deformed Hartree–Fock–Bogolyubov calculations, distorted wave Born approximation

(Some figures may appear in colour only in the online journal)

1. Introduction

Electron scattering plays a significant role in studying nuclear electromagnetic structures [1–6]. In past decades, plenty of electron scattering experiments have been performed on stable nuclei and a large amount of nuclear information has been accurately extracted, such as the charge radii and charge density distributions [7, 8]. There are two main benefits to use the electron as probes. On one hand, the basic theory of electromagnetic interaction between electron and nuclei is well understood. By the electron scattering, the theoretical uncertainties in the data analysis can be significantly eliminated. On the other hand, compared with the strong interaction, the electromagnetic interaction is much weaker, which means the properties of the nuclei can hardly be influenced.

In recent years, on account of the new experimental phenomena discovered in exotic nuclei, the researches on the structures of unstable nuclei have increasingly become a hot point in nuclear physics [9–12], for example the neutron skin, the proton halo, and the bubble nuclei [13–16]. It has been received considerable attention to investigate the nuclear structure of short-lived nuclei by the electron scattering. For this purpose, the new-generation radioactive isotope facilities are constructed at RIKEN [17–19] and GSI [20, 21]. The new technique self-confining radioactive-isotope ion target can perform the ion-trapping phenomenon in electron storage ring, and produce the exotic nuclei in $A = 130$ region of nuclear chart [22]. The first elastic electron scattering experiment has been finished on the nucleus ^{132}Xe recently [19]. With the new facilities, the structure of nuclei far from the β-stable line can be measured by the electron scattering in the future.

In order to better interpret the experimental data, many theoretical models are developed accordingly to calculate the electron scattering form factors. The plane-wave Born approximation (PWBA) is considered as a convenient method [2, 3], which expresses the scattering form factors as the Fourier transformation of the charge density distributions. However, the PWBA calculations are not accurate enough, because the nuclear Coulomb distortion effects are neglected when applied to the heavy nuclei. In order to obtain more precise results, the distorted wave Born approximation (DWBA) method is developed where the nuclear Coulomb distortion effects on wave functions of scattered electron are taken into account [23–25].

With the DWBA method, the charge form factors $|F_C(q)|^2$ have been systematically investigated where the corresponding charge density distributions are calculated from a variety of different nuclear structure models, such as the relativistic-mean-field (RMF) model, the shell model, the Hartree–Fock–Bogolyubov (HFB) model and the three body model [9, 26–36]. By comparing the theoretical results with the experimental data, the validity and suitability of the nuclear structure models can be examined. Nevertheless, for some nuclei, there are deviations between the theoretical $|F_C(q)|^2$ and experimental data. This is due to the assumption of the spherical symmetry during the calculations. It has been proved experimentally and theoretically that most nuclei are deformed [37–40]. The influences of deformation on electron scattering are first discussed in [41, 42]. In recent researches [43, 44], the authors developed the scattering models by combining the deformed RMF model and the DWBA method. Based on the deformed scattering model, the $|F_C(q)|^2$ of even–even nuclei and odd-A nuclei are calculated.

Apart from the RMF model, the deformed HFB method is also extensively applied in studying the nuclear properties of exotic nuclei. For instance, the nuclear energies of spherical and deformed nuclei, the structure of halo nuclei and weakly bound nuclei are investigated in [45–49]. By the electron scattering, the nuclear density distributions and single particle wave functions from deformed HFB model can also be discussed. In recent paper [50], the authors calculated the magnetic form factors within the deformed HFB model for the first time. By comparing the theoretical results with the experimental data, the reliability of single-particle wave functions obtained by the deformed HFB model are demonstrated.

Based on previous researches, we further extend the studies of the nuclear charge form factors $|F_C(q)|^2$ to the region of deformed HFB calculations. A developed scattering model is constructed by combining the deformed HFB model and the DWBA method. Some typical spherical and deformed nuclei are chosen as the candidates. Comparing the theoretical $|F_C(q)|^2$ with experimental data, the reliability of the deformed HFB model to describe the charge density distributions can be verified. Next, the $|F_C(q)|^2$ of the even–even Xe isotopes and odd-A Cs isotopes are systematically calculated. By further constraining the nuclei to certain shapes, the influences of the nuclear deformation on $|F_C(q)|^2$ of isotopic chains can be analyzed. For even–even Xe isotopes, the positions of the diffraction minima of $|F_C(q)|^2$ have noticeable distinctions when the deformation parameter β_2 increases. For odd-A Cs isotopes, the values of the diffraction minima of $|F_C(q)|^2$ are sensitively influenced by different β_2. The electron scattering experiments off exotic nuclei have been carried out successfully in RIKEN recently [19]. With the studies in this paper, the Coulomb form factors of unstable isotopes can be analyzed in advance, which can provide an effective guide for the scattering experiments in the future.

The paper is organized as follows: in section 2, the theoretical framework for the HFB model and DWBA method is provided. In section 3, the numerical results and discussions are presented. Finally, a summary is given in section 4.

2. Theoretical framework

In this section, the developed scattering model is constructed by combing the axially deformed solutions of HFB model and DWBA method. The corresponding formalism for the Coulomb form factors is presented.

2.1. Axially deformed HFB model

For the Skyrme force, the energy density functional can be written as the sum of the mean-field and pairing energy densities [51]

$$\mathcal{H}(\mathbf{r}) = H(\mathbf{r}) + \tilde{H}(\mathbf{r}), \tag{1}$$

where

$$H(\mathbf{r}) = \frac{\hbar^2}{2m}\tau + \frac{1}{2}t_0\left[\left(1+\frac{1}{2}x_0\right)\rho^2 - \left(\frac{1}{2}+x_0\right)\sum_q \rho_q^2\right] + \frac{1}{2}t_1\left[\left(1+\frac{1}{2}x_1\right)\rho\left(\tau - \frac{3}{4}\Delta\rho\right) - \left(\frac{1}{2}+x_1\right)\sum_q \rho_q\left(\tau_q - \frac{3}{4}\Delta\rho_q\right)\right]$$

$$+\frac{1}{2}t_2\left[\left(1+\frac{1}{2}x_2\right)\rho\left(\tau+\frac{1}{4}\Delta\rho\right)-\left(\frac{1}{2}+x_2\right)\sum_q\rho_q\left(\tau_q+\frac{1}{4}\Delta\rho_q\right)\right]$$
$$+\frac{1}{12}t_3\rho^\alpha\left[\left(1+\frac{1}{2}x_3\right)\rho^2-\left(x_3+\frac{1}{2}\right)\sum_q\rho_q^2\right]$$
$$-\frac{1}{8}(t_1x_1+t_2x_2)\sum_{ij}\mathbf{J}_{ij}^2+\frac{1}{8}(t_1-t_2)\sum_q\mathbf{J}_{q,ij}^2$$
$$-\frac{1}{2}W_0\sum_{ijk}\varepsilon_{ijk}\left[\rho\nabla_k\mathbf{J}_{ij}+\sum_q\rho_q\nabla_k\mathbf{J}_{q,ij}\right], \tag{2}$$

and

$$\tilde{H}(\mathbf{r})=\frac{1}{2}V_0\left[1-V_1\left(\frac{\rho}{\rho_0}\right)^\gamma\right]\sum_q\tilde{\rho}_q^2. \tag{3}$$

By the variation of the HFB energy, the HFB equation can be obtained as

$$\sum_{\sigma'}\begin{pmatrix}h(\mathbf{r},\,\sigma,\,\sigma') & \tilde{h}(\mathbf{r},\,\sigma,\,\sigma')\\ \tilde{h}(\mathbf{r},\,\sigma,\,\sigma') & -h(\mathbf{r},\,\sigma,\,\sigma')\end{pmatrix}\begin{pmatrix}U(E,\,\mathbf{r}\sigma')\\ V(E,\,\mathbf{r}\sigma')\end{pmatrix}=\begin{pmatrix}E+\lambda & 0\\ 0 & E-\lambda\end{pmatrix}\begin{pmatrix}U(E,\,\mathbf{r}\sigma)\\ V(E,\,\mathbf{r}\sigma)\end{pmatrix}. \tag{4}$$

For axially symmetric deformed nuclei, the quasiparticle HFB states can be characterized by eigenvalue Ω_i of the third component J_z of the total angular momentum:

$$\begin{pmatrix}U_k(\mathbf{r},\,\sigma,\,\tau)\\ V_k(\mathbf{r},\,\sigma,\,\tau)\end{pmatrix}=\chi_{q_k}(\tau)\left[\begin{pmatrix}U_k^+(r,\,z)\\ V_k^+(r,\,z)\end{pmatrix}\mathrm{e}^{\mathrm{i}\Lambda^-\varphi}\chi_{+1/2}(\sigma)+\begin{pmatrix}U_k^-(r,\,z)\\ V_k^-(r,\,z)\end{pmatrix}\mathrm{e}^{\mathrm{i}\Lambda^+\varphi}\chi_{-1/2}(\sigma)\right], \tag{5}$$

where $\Lambda^\pm=\Omega_k\pm1/2$.

The upper and lower components of the quasiparticle states are further expanded by the eigenfunctions of the axially deformed harmonic-oscillator potential with the quantum numbers $\alpha=\{n_r,\,n_z,\,\Lambda,\,\Sigma\}$,

$$U_k(\mathbf{r},\,\sigma,\,\tau)=\chi_{q_k}(\tau)\sum_\alpha U_{k\alpha}\Phi_\alpha(\mathbf{r},\,\sigma),$$
$$V_k(\mathbf{r},\,\sigma,\,\tau)=\chi_{q_k}(\tau)\sum_\alpha V_{k\alpha}\Phi_\alpha(\mathbf{r},\,\sigma), \tag{6}$$

where n_r and n_z represent the numbers of nodes in r and z directions, respectively, and Λ and Σ represent the projections of the angular momentum and the spin along the symmetry axis.

The local densities can be calculated from the quasiparticle HFB solutions [52, 53]

$$\rho(r,\,z)=\sum_k(|V_k^+(r,\,z)|^2+|V_k^-(r,\,z)|^2). \tag{7}$$

Combining the equations (4)–(7), the HFB equations can be solved iteratively until the desired accuracy is achieved.

During the calculations, the Bogolyubov approximation does not conserve the particle number, therefore the particle-number projection operator is included in the model to restore the particle number symmetries

$$P^N=\frac{1}{2\pi}\int\mathrm{d}\phi\mathrm{e}^{\mathrm{i}\phi(\hat{N}-N)}, \tag{8}$$

where $\hat{N}$ denotes the number operator. In order to obtain the potential energy surface along the quadrupole moments, the HFB energies at certain deformation are also constrained by an unrestricted variation of the function during the calculations:

$$E^{Q} = C_{Q}(\langle\hat{Q}\rangle - \overline{Q})^{2}. \tag{9}$$

$\langle\hat{Q}\rangle$ is the expectation value of the quadrupole moment, and C_Q is the stiffness constant.

2.2. Nuclear Coulomb form factors

From the HFB equation, the accurate density distributions can be obtained. Neglecting the effect of the neutron contributions, the charge density distributions $\rho_c(r)$ can be derived by integrating the single-proton charge distributions [54]

$$\rho_{c}(\mathbf{r}) = \int \rho_{p}(\mathbf{r}')\rho^{p}(|\mathbf{r} - \mathbf{r}'|)\mathrm{d}\mathbf{r}', \tag{10}$$

where $\rho^{p}(r) = \frac{\Lambda^{3}}{8\pi}\mathrm{e}^{-\Lambda r}$ with $\Lambda = 842.61$ MeV.

The deformed charge densities are further expanded into the multipole moment distributions by the Legendre function [55]

$$\rho_{c}(r, z) = \sum_{k} \rho_{k}(R)P_{k}(\cos\theta) = \rho_{0}(R) + \rho_{2}(R)P_{2}(\cos\theta) + \cdots, \tag{11}$$

where

$$\rho_{k}(R) = \frac{2k+1}{2}\int_{-1}^{1} P_{k}(\cos\theta)\rho(R\cos\theta, R\sin\theta)\mathrm{d}(\cos\theta). \tag{12}$$

The $\rho_0(R)$ represents the spherical part of charge distribution and $\rho_2(R)$ provides the nuclear quadrupole distribution.

With the density multipoles $\rho_k(R)$, the nuclear Coulomb form factors $|F_C(q)|^2$ can be investigated. In the PWBA method, $|F_C(q)|^2$ are simply calculated from the charge densities via the Fourier transform

$$F_{C}(q) = \frac{1}{Z}\int \rho_{c}(\mathbf{r})\mathrm{e}^{\mathrm{i}\mathbf{q}\cdot\mathbf{r}}\,\mathrm{d}\mathbf{r}. \tag{13}$$

Substituting the equation (11) into equation (13), the Coulomb form factors can be decomposed into several Coulomb multipoles [42]

$$|F_{C}(q)|^{2} = \sum_{\lambda=0,2,\cdots}^{2J} |F^{C\lambda}(q)|^{2}. \tag{14}$$

The Coulomb multipoles can be derived by the intrinsic multipoles

$$F^{C\lambda} = \langle Jk\lambda 0|J\lambda Jk\rangle \mathscr{F}^{C\lambda}, \tag{15}$$

where the intrinsic multipoles $\mathscr{F}^{C\lambda}$ reflect the contributions of the charge density multipoles

$$\mathscr{F}^{C\lambda} = \frac{4\pi}{Z\sqrt{2\lambda+1}}\int r^{2}\rho_{\lambda}(r)j_{\lambda}(qr)\mathrm{d}r. \tag{16}$$

The Clebsch–Gordan (CG) coefficient $\langle Jk\lambda 0|J\lambda Jk\rangle$ provides the weights of different intrinsic multipoles, and the k is the total spin projection along the symmetry axis.

With the PWBA method, the nuclear Coulomb form factors can be obtained conveniently, which is beneficial for the physical discussions. However, the results of the PWBA method are not accurate enough, due to the lack of the nuclear Coulomb distorted effects.

Therefore, the influences of nuclear Coulomb distortions are further included by the DWBA calculations.

For the $C0$ multipole, which represents the contributions of spherical parts of charge densities, the distorted wave function of scattered electron can be obtained by solving the Dirac equation with a spherical Coulomb potential $V_c(r)$ from the $\rho_0(r)$

$$[\boldsymbol{\alpha}\cdot\boldsymbol{p}+\beta m+V_c(r)]\Psi(\mathbf{r})=E\Psi(\mathbf{r}). \tag{17}$$

With the distorted wave function, the direct scattering amplitude $f(\theta)$ and spin-flip scattering amplitude $g(\theta)$ can be derived, and the $C0$ multipole can be written as

$$F^{C0}(q)=(|f(\theta)|^2+|g(\theta)|^2)/\sigma_{\mathrm{Mott}}, \tag{18}$$

where σ_{Mott} is the Mott scattering cross section.

The deformations of most nuclei are not large, therefore, the $C0$ multipoles occupy the major parts of the Coulomb form factors, which are calculated precisely by the DWBA method. The higher multipoles $C\lambda$ represent the contributions of deformed parts of charge densities, which only influence the positions of the diffraction minima of Coulomb form factors $|F_C(q)|^2$. Compared with total Coulomb form factors, the values of $C2$ multipoles are small enough, which can be seen in figure 1 of [56] and figure 11(b) of this paper. Therefore, the effects of coulomb distortions and the interferences between the Coulomb distortions and deformation can be neglected for $C2$ multipoles. Instead of DWBA method, the PWBA method are used to calculate the higher multipoles $C\lambda$, and the corresponding coulomb distortions of higher multipoles are taken into account from a simple prescription by replacing the momentum transfer q with the effective momentum transfer q_{eff} [50].

$$q_{\mathrm{eff}}=q[1+1.5\alpha Z\hbar c/(ER_0)], \tag{19}$$

where $R_0=1.20A^{1/3}$ and A is the mass number of nucleus. Combining the equations (14)–(19), the nuclear Coulomb form factor $|F_C(q)|^2$ can be obtained.

3. Numerical results and discussion

In this section, the Coulomb form factors $|F_C(q)|^2$ of the even–even nuclei and odd-A nuclei are calculated with the formulas of section 2.

3.1. $|F_C(q)|^2$ for representative nuclei

We first present the theoretical binding energies per nucleon B/A (MeV), charge root-mean-square (RMS) radii R_C (fm) and deformation parameters β_2 for both the spherical and deformed nuclei in table 1, which are calculated by the spherical and axially deformed HFB model with the SLY4 parameter set. From table 1, one can see that both the spherical and deformed HFB model can provide robust descriptions for the binding energies and charge radii. Besides, the deformed HFB model can also give reasonable deformation parameters β_2.

The charge RMS radii R_C only describe the nuclear electromagnetic properties roughly. Compared with the charge radii R_C, the nuclear electromagnetic structures can be reflected by $|F_C(q)|^2$ more exactly. Therefore, the theoretical $|F_C(q)|^2$ for nuclei in table 1 are calculated with the density distributions from the spherical and deformed HFB model, and the results are compared with each other.

3.1.1. Spherical nuclei. Decomposing the charge density $\rho_c(r,z)$ from the axially deformed HFB model with equations (11) and (12), the multipole moment of charge distributions $\rho_k(r)$

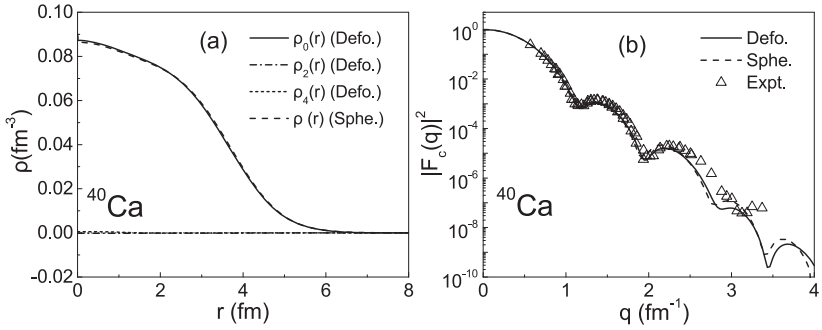

Figure 1. (a) Charge density multipoles $\rho_k(r)$ of ^{40}Ca from the deformed HFB model and the charge distributions $\rho(r)$ from the spherical HFB model. (b) Coulomb form factors $|F_C(q)|^2$ of ^{40}Ca calculated from spherical and deformed HFB densities. The experimental data are taken from the [59].

Table 1. Theoretical binding energies per nucleon B/A (MeV), charge RMS radii R_C (fm), and deformation parameters β_2 for the candidate nuclei, calculated by the spherical and axially deformed HFB model with the SLY4 parameter set. The experimental data are taken from the [8, 57, 58].

Nuclei	Model	B/A	R_C	β_2
^{40}Ca	Sphe.	−8.62	3.51	0.00
	Defo.	−8.64	3.50	0.00
	Expt.	−8.55	3.48	0.12
^{208}Pb	Sphe.	−7.86	5.52	0.00
	Defo.	−7.87	5.52	0.00
	Expt.	−7.87	5.50	0.05
^{52}Cr	Sphe.	−8.77	3.67	0.00
	Defo.	−8.79	3.70	0.14
	Expt.	−8.78	3.65	0.22
^{132}Xe	Sphe.	−8.40	4.79	0.00
	Defo.	−8.41	4.81	0.12
	Expt.	−8.43	4.79	0.14

of ^{40}Ca and ^{208}Pb are calculated and presented in figures 1(a) and 2(a). It can be seen that the spherical part $\rho_0(r)$ is the major part while the quadrupole distributions $\rho_2(r)$ and hexadecapole distributions $\rho_4(r)$ are close to zero. For comparison, $\rho(r)$ from the spherical HFB model are also presented in the figures 1(a) and 2(a). There are only tiny differences between the spherical component $\rho_0(r)$ and $\rho(r)$. Therefore, for the case of spherical nuclei, the deformed HFB densities can return to the results of spherical HFB model.

With the charge distributions in figure 1(a), the Coulomb form factors $|F_C(q)|^2$ of ^{40}Ca are further calculated by the DWBA method, and the results are given in figure 1(b). The experimental data are also given in this figure for comparison. As shown in figure 1(b), the $|F_C(q)|^2$ from the deformed and spherical HFB densities are almost coincident exactly with each other, and both of them agree with the experimental data. This is due to the $\rho_2(r)$ and $\rho_4(r)$ of spherical nuclei are close to zero, which can be reflected in the figure 1(a). Besides, there are almost no differences between the $\rho_0(r)$ from the deformed HFB model and $\rho(r)$

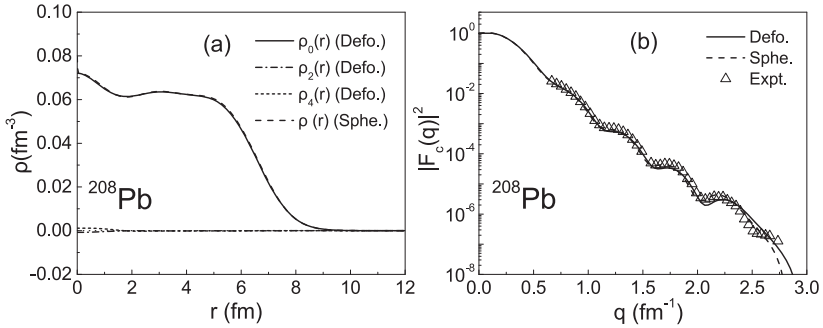

Figure 2. Same as the figure 1, but for ^{208}Pb. The experimental data are taken from the [60].

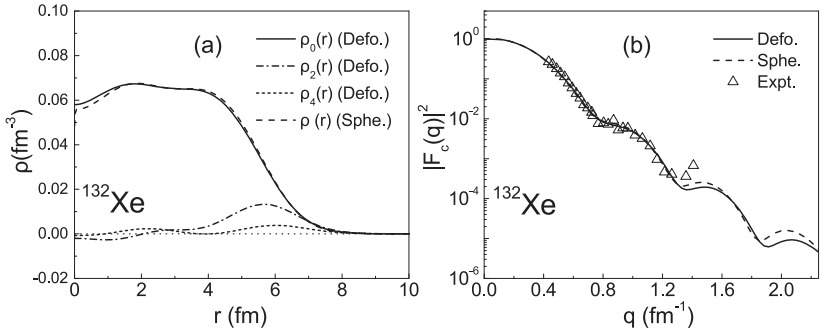

Figure 3. (a) Multipole charge density distributions for ^{132}Xe from the deformed HFB model. $\rho(r)$ from the spherical HFB model are also presented for comparison. (b) The nuclear Coulomb form factors of ^{132}Xe are calculated from the spherical and deformed HFB densities. The experimental data are taken from the [19].

from the spherical HFB model. Therefore, the corresponding $|F_C(q)|^2$ in figure 1(b) are very close to each other.

Besides ^{40}Ca, the $|F_C(q)|^2$ of ^{208}Pb are also calculated with the DWBA method, and the results are presented in the figure 2(b). In this figure, the theoretical $|F_C(q)|^2$ from the deformed HFB densities and spherical HFB densities agree with the experimental data, which can be attributed to the similarity between the $\rho_0(r)$ and $\rho(r)$ in figure 2(a). The figures 1(a) and 2(a) show that the deformed HFB model is a more general method and contains the solutions of the spherical HFB model. Moreover, the deformed HFB model can provide reasonable descriptions for the charge distributions of spherical nuclei.

3.1.2. Deformed nuclei. Besides the spherical nuclei, the theoretical $|F_C(q)|^2$ of the deformed nuclei in table 1 are also calculated in this paper. The multipole charge density distributions of ^{132}Xe are shown in figure 3(a), which are investigated by the deformed HFB model with the SLY4 parameter set. For comparison, the charge density distributions $\rho(r)$ obtained from the spherical HFB model are also given in this figure. In figure 3(a), the spherical part $\rho_0(r)$ plays a major role in the contributions of charge distributions, though ^{132}Xe has a deformation of $\beta_2 = 0.12$. Compared with the spherical part $\rho_0(r)$, the quadrupole distribution $\rho_2(r)$ is much smaller. As the multipole order k increases, the values of the ρ_k decrease rapidly. For $k > 4$,

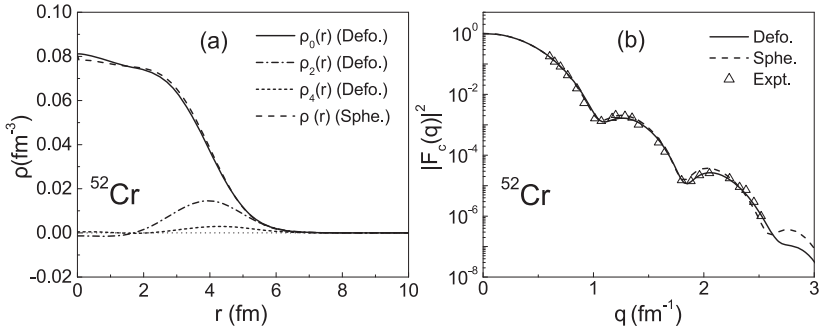

Figure 4. Same as the figure 3, but for ^{52}Cr. The experimental data are taken from the [61].

the multipole components ρ_k can be neglected. Because of the existence of ρ_2 multipole, there are definite differences between $\rho_0(r)$ from the deformed HFB model and $\rho(r)$ from the spherical HFB model.

The $|F_C(q)|^2$ of ^{132}Xe are calculated with the charge density distributions in figure 3(a) and compared with the latest experimental data in figure 3(b). In this figure, the theoretical $|F_C(q)|^2$ of ^{132}Xe investigated by the spherical and the deformed scattering model are similar to each other, and both of them coincide with the experimental data. At the second diffraction minimum ($q \approx 1.3$ fm^{-1}), there are differences between the spherical and deformed results. This is owing to the distinction of the $\rho_0(r)$ and $\rho(r)$ in figure 3(a).

The charge density distributions of ^{52}Cr from the deformed HFB model are also investigated and decomposed into different multipole components ρ_k in figure 4(a). The values of $\rho_2(r)$ of ^{52}Cr and ^{132}Xe are similar, because of the almost identical deformation parameters β_2 in table 1. With the charge density distributions in figure 4(a), the $|F_C(q)|^2$ of ^{52}Cr are calculated and presented in figure 4(b). As shown in figure 4(b), the theoretical $|F_C(q)|^2$ from the deformed HFB charge density are in better agreement with the experimental data. The results of figures 1–4 indicate that the deformed HFB model can well describe the nuclear charge distributions for both the spherical and deformed nuclei. The nuclear charge form factors can be investigated by combing the deformed HFB model and the DWBA method.

3.2. Investigations on even–even Xe isotopes

In this part, the Coulomb form factors $|F_C(q)|^2$ of even–even isotopic chains are studied by combining the deformed HFB model and the DWBA method. Analyzing the diffraction minima of the $|F_C(q)|^2$ of isotopic chain, the influences of nuclear deformation on the structures of nuclei can be reflected.

The theoretical binding energies per nucleon B/A and charge RMS radii R_C of Xe isotopes are first calculated by the spherical and deformed HFB model, and the results are presented in figure 5. From this figure, one can see that compared with the spherical HFB model, the calculations from the deformed HFB model coincide with the experimental data better. For charge radii R_C in figure 5(b), the deformed results are larger than the spherical one. This phenomenon can attribute to the connection between deformed and spherical radius [62]

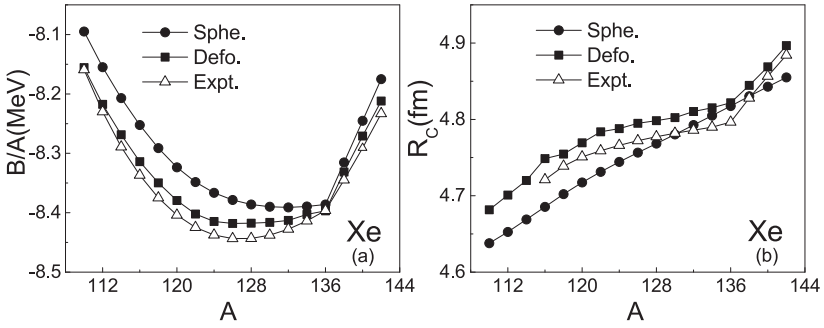

Figure 5. Binding energies per nucleon B/A (MeV) and charge RMS radii R_C (fm) for Xe isotopes from the spherical and deformed HFB model with the SLY4 parameter set. The experimental data are taken from the [8, 58].

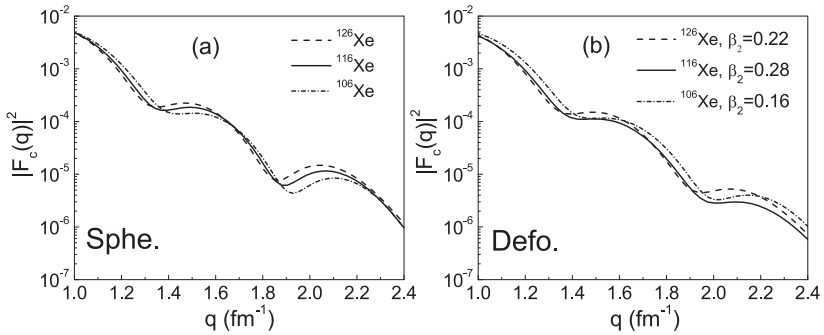

Figure 6. (a) $|F_C(q)|^2$ of ^{106,116,126}Xe calculated by the spherical scattering model. (b) $|F_C(q)|^2$ of ^{106,116,126}Xe calculated by the deformed scattering model.

$$R^2 = R^2_{\text{sphe}}\left(1 + \frac{5}{4\pi}\beta_2^2\right), \tag{20}$$

where the R_{sphe} is the spherical radius and is proportional to $A^{1/3}$.

Besides the B/A and R_C, the Coulomb form factors $|F_C(q)|^2$ of Xe isotopes are also investigated. In figure 6(a), we present the DWBA form factors from the spherical HFB model. The positions of diffraction minima play a significant role in studying the Coulomb form factors of isotopic chain. It can be seen that the Coulomb form factors of ^{106}Xe, ^{116}Xe and ^{126}Xe in figure 6(a) are close to each other. With the increase of mass number A, the diffraction minima of the Coulomb form factors move inward, which has been discussed in previous researches [27, 29, 30].

For comparison, the DWBA form factors of ^{106}Xe, ^{116}Xe and ^{126}Xe obtained from the deformed HFB model are presented in the figure 6(b). Compared with the results in figure 6(a), the $|F_C(q)|^2$ in figure 6(b) are much different. Instead of the inward shifts with increasing of mass number A in figure 6(a), the diffraction minima of ^{116}Xe locate at the same positions as those of ^{106}Xe. Besides, the $|F_C(q)|^2$ of ^{116}Xe are smaller than the ^{106}Xe on the whole. These differences are owing to the nuclear deformation. For ^{106}Xe with small deformation parameter $\beta_2 = 0.16$, the $|F_C(q)|^2$ from the spherical and deformed calculations are almost the same in figures 6(a) and (b). However, for ^{116}Xe with $\beta_2 = 0.28$, there are distinct downward and outward trends for the $|F_C(q)|^2$ from the deformed HFB model.

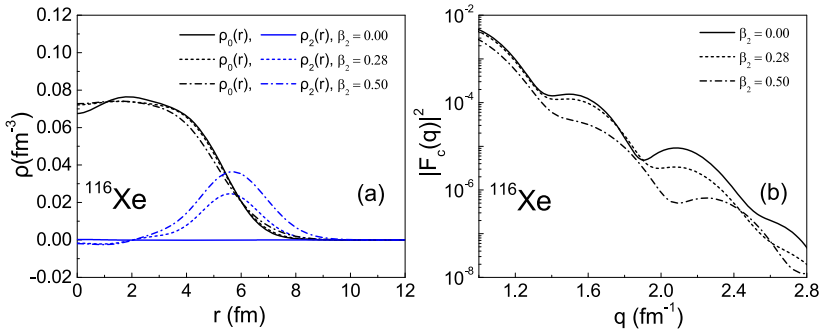

Figure 7. (a) Charge density multipoles of ^{116}Xe for deformation parameter $\beta_2 = 0.00$, 0.28 and 0.50 from the constrained HFB calculations, respectively. (b) The corresponding DWBA form factors of ^{116}Xe with different deformation parameters.

In order to analyze the influences of the nuclear deformation on $|F_C(q)|^2$, the charge density multipoles of ^{116}Xe from the constrained HFB calculations ($\beta_2 = 0.00$, 0.28 and 0.50) are presented in figure 7(a). There are noticeable distinctions of the $\rho_0(r)$ with different β_2 in figure 7(a). When the deformation parameter β_2 increases, the deformed parts $\rho_2(r)$ become lager and the shape of $\rho_0(r)$ also changes. With the charge density multipoles in figure 7(a), the corresponding DWBA Coulomb form factors are presented in figure 7(b). One can see that the positions of the diffraction minima of the $|F_C(q)|^2$ have downward and outward shifts, as the deformation parameter β_2 increases. Therefore, by measuring the positions of diffraction minima, the influences of nuclear deformation on $|F_C(q)|^2$ can be reflected.

It should be mentioned that the influences of the nuclear deformations on $|F_C(q)|^2$ have been analyzed in [43] based on deformed RMF calculations. In figures 6 and 7 of this paper, the similar results are obtained from the deformed HFB calculations, which are consistent with previous researches. This means both the RMF model and HFB model can well describe the nuclear electromagnetic structures. However, due to the lack of experimental data of neutron radii in the process of building models, the RMF and HFB models lead to very different nuclear neutron properties and slope parameters of symmetry energy [63–65]. These differences can be further analyzed by the parity violating electron scattering and other methods. Combining the previous studies and the results of this paper, it can be concluded that for electron scattering off isotopic chain, the influences of deformation need to be considered. Recently, the electron scattering experiments of ^{132}Xe have been performed in RIKEN. If the electron scattering experiments on other unstable Xe isotopes are carried out in the future, the effects of nuclear deformation cannot be ignored.

3.3. Investigations on the odd-A Cs isotopes

Apart from the even–even Xe isotopic chain, we also choose the Cs isotopes to investigate the Coulomb form factors $|F_C(q)|^2$ of odd-A nuclei. The electron scattering experiment of ^{137}Cs will be carried out in the coming future in RIKEN. The corresponding theoretical investigations are useful to guide the experimental measurements and interpret the experimental data.

Similar to the studies of Xe isotopes, we first present the theoretical binding energies per nucleon B/A and charge RMS radii R_C of Cs isotopes in figure 8, respectively. Comparing with the spherical HFB model, the theoretical results from the deformed HFB model show

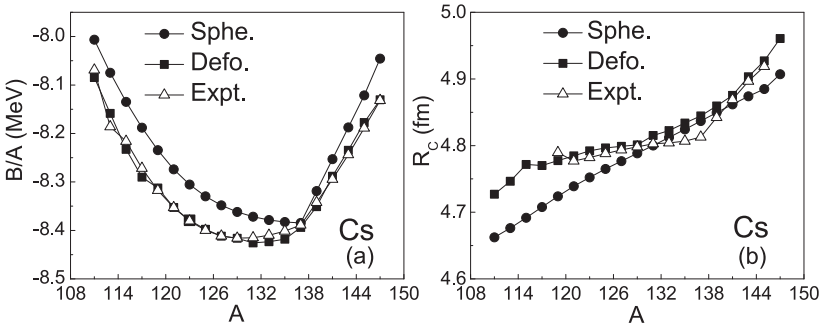

Figure 8. Binding energies per nucleon B/A (MeV) and charge RMS radii R_C (fm) for Cs isotopes calculated by the spherical and deformed HFB model with the SLY4 parameter set. The experimental data are taken from the [8, 58].

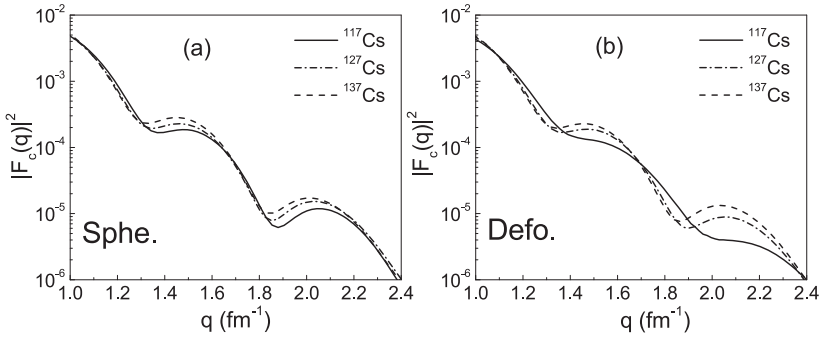

Figure 9. (a) $|F_C(q)|^2$ of ^{117,127,137}Cs calculated by the spherical scattering model. (b) $|F_C(q)|^2$ of ^{117,127,137}Cs calculated by the deformed scattering model.

better agreement with experimental data. Figure 8 shows that the ground properties of odd-A nuclei can be well described by the deformed HFB model.

In addition to B/A and R_C, the $|F_C(q)|^2$ of the odd-A Cs isotopic chain are further calculated to give a more detailed description on the nuclear electromagnetic structures. Unlike the even–even Xe isotopes, the angular momentum of the ground state of odd-A Cs isotopes is $J^\pi \neq 0$. With the equation (14), the $|F_C(q)|^2$ of Cs isotopes contain not only the multiples $C0$, but also higher multipoles $C2$ and $C4$.

In figure 9(a), we first provide the DWBA form factors of Cs isotopes from the spherical HFB calculations, whose changing trends are similar to Xe isotopes in figure 6(a). With the increase of the mass number A, the diffraction minima of the $|F_C(q)|^2$ shift inward. This is because the charge distributions of spherical HFB model only contain the spherical part $\rho_0(r)$ and lack the higher multipoles $\rho_2(r)$ and $\rho_4(r)$. Therefore, there are no significant changes between the results of figures 6(a) and 9(a). By combining the deformed HFB model and DWBA method, the nuclear deformations are taken into account to investigate the $|F_C(q)|^2$, and the results are presented in figure 9(b). As shown in figure 9(b), there are marked changes in the shape and the variation tendency of the $|F_C(q)|^2$. As the deformation parameter β_2 increases, the corresponding $|F_C(q)|^2$ gradually become flat. For ^{117}Cs with the biggest nuclear deformation $\beta_2 = 0.26$, there is no obvious diffraction minimum for the $|F_C(q)|^2$.

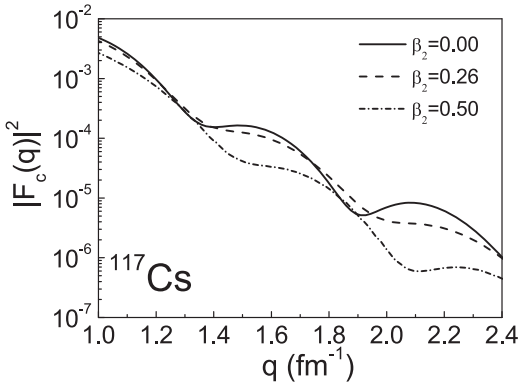

Figure 10. $|F_C(q)|^2$ of ^{117}Cs for deformation parameter $\beta_2 = 0.00$, 0.26 and 0.50 calculated by DWBA method, where the corresponding $\rho_c(r)$ are obtained by the constrained HFB calculations.

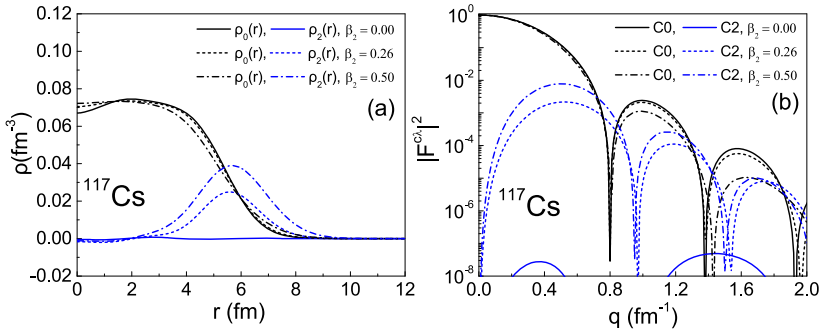

Figure 11. (a) Charge density multipoles of ^{117}Cs for $\beta_2 = 0.00$, 0.26 and 0.50 from the constrained HFB calculations. (b) The corresponding Coulomb multipoles C_0^2 and C_2^2 of different deformation parameters β_2 of ^{117}Cs.

To further analyze the effects of nuclear deformation on the diffraction minima of figure 9(b), the $|F_C(q)|^2$ of ^{117}Cs from the constrained HFB calculations with different deformation parameters β_2 are presented and compared in figure 10. With the increase of β_2, the diffraction minima of $|F_C(q)|^2$ gradually become flat, which are similar to the results mentioned above. To illustrate the changing trends of $|F_C(q)|^2$ in figure 10, the charge density multipoles from constrained HFB calculations are given in figure 11(a). For ^{117}Cs with $\beta_2 = 0.50$, the deformed multipole density $\rho_2(r)$ is the largest. The corresponding Coulomb multipoles $C0$ and $C2$ are also presented in figure 11(b). Compared with the $C0$ multipole, the $C2$ multipole is much smaller in most momentum transfers. However, at the diffraction minima of $C0$ multipole, the $C2$ multipole cannot be ignored. The angular momentum of the ground state of ^{117}Cs is $J^\pi = \frac{9^+}{2}$, and its $|F_C(q)|^2$ contain $C0$ and the higher multipoles from equation (14). Taking into account the contributions of deformed parts $\rho_2(r)$ of density distributions, the $|F_C(q)|^2$ of ^{117}Cs in figure 10 become flat and do not have obvious minima. Combining figures 9 and 10, we can draw a conclusion that the nuclear deformation can influence the values of the diffraction minima of the $|F_C(q)|^2$ for odd-A Cs isotopes. With the increase of β_2, the diffraction minima of the $|F_C(q)|^2$ fade away. Both theoretical and experimental investigations have indicated that most of Cs

isotopes are deformed [37, 39]. Therefore, the nuclear deformation needs to be taken into account in the studies of electron scattering off odd-*A* nuclei.

It should also be mentioned that, for the odd-*A* nuclei ^{127}Cs and ^{137}Cs, there still are diffraction minima in figure 9(b). The angular momentum of ^{127}Cs is $J^{\pi} = \frac{1^{+}}{2}$, and from the equation (14) it only contains the $C0$ multipole. For the ^{137}Cs, the angular momentum is $J^{\pi} = \frac{7^{+}}{2}$ and its form factors have the $C0$, $C2$ and $C4$ multipoles. However, ^{137}Cs is a magic-number nucleus with the $\beta_2 = 0.0$ from the deformed HFB calculations, and its $C2$ and $C4$ multipoles can be neglected.

4. Summary and conclusion

The Coulomb form factors $|F_C(q)|^2$ are significant to investigate the nuclear electromagnetic structure. In previous studies, the deformed RMF model and the DWBA method were combined to calculate the $|F_C(q)|^2$. In this paper, we further extend the studies of $|F_C(q)|^2$ with the deformed HFB model and DWBA method.

With the DWBA method, the theoretical Coulomb form factors of both the spherical nuclei (^{40}Ca and ^{208}Pb) and deformed nuclei (^{132}Xe and ^{52}Cr) are calculated, where the corresponding charge densities are obtained from the deformed HFB calculations, respectively. Results indicate that the deformed HFB model can provide reasonable descriptions on the nuclear density distributions of both the spherical and deformed nuclei.

Combining the HFB model and DWBA method, the $|F_C(q)|^2$ of the isotopic chains are also calculated to study the influences of nuclear deformation on the $|F_C(q)|^2$ of isotopic chain. For even–even Xe isotopes, the nuclear deformation can influence the positions of the diffraction minima of $|F_C(q)|^2$. With the increase of deformation parameter β_2, the diffraction minima of $|F_C(q)|^2$ have noticeable downward and outward shifts. For odd-*A* Cs isotopes, the values of the diffraction minima of $|F_C(q)|^2$ can be sensitively affected by the nuclear deformation. The $|F_C(q)|^2$ become flat and do not have obvious minima, when the β_2 increases. The electron scattering experiments of Xe isotopes and Cs isotopes have been finished or will be started in the near future in RIKEN. The methods proposed in this paper can offer effective guides for the coming experiments and can also be used to interpret the experimental data.

Acknowledgments

This work is supported by the National Natural Science Foundation of China (Grants Nos. 11505292, 11535004, 11822503, 11575082, and 11605105), by the Fundamental Research Funds for the Central Universities (Grant Nos. 17CX02044 and 15CX07005A), and by the China Scholarship Council (CSC).

ORCID iDs

Jian Liu https://orcid.org/0000-0001-6546-6838

References

[1] Hofstadter R 1956 *Rev. Mod. Phys.* **28** 214
[2] Willey R S 1963 *Nucl. Phys.* **40** 529
[3] de Forest T and Walecka J D 1966 *Adv. Phys.* **15** 1

[4] Überall H 1971 *Electron Scattering from Complex Nuclei* (New York: Academic)
[5] Walecka J D 2001 *Electron Scattering for Nuclear and Nucleon Structure* (Cambridge: Cambridge University Press)
[6] Sick I and Trautmann D 2014 *Phys. Rev.* C **89** 012201
[7] De Vries H, De Jager C W and De Vries C 1987 *At. Data Nucl. Data tables* **36** 495
[8] Angeli I and Marinova K P 2013 *At. Data Nucl. Data tables* **99** 69
[9] Garrido E and Moya de Guerra E 1999 *Nucl. Phys.* A **650** 387
[10] Suda T and Wakasugi M 2005 *Prog. Part. Nucl. Phys.* **55** 417
[11] Suda T 2011 *J. Phys.:Conf. Ser.* **267** 012008
[12] Lyu M, Yoshida K, Kanada-En'yo Y and Ogata K 2018 *Phys. Rev.* C **97** 044612
[13] Minamisono T *et al* 1992 *Phys. Rev. Lett.* **69** 2058
[14] Centelles M, Roca-Maza X, Viñas X and Warda M 2009 *Phys. Rev. Lett.* **102** 122502
[15] Grasso M *et al* 2009 *Phys. Rev.* C **79** 034318
[16] Meucci A, Vorabbi M, Giusti C and Finelli P 2014 *Phys. Rev.* C **90** 027301
[17] Wakasugi M *et al* 2008 *Phys. Rev. Lett.* **100** 164801
[18] Suda T *et al* 2009 *Phys. Rev. Lett.* **102** 102501
[19] Tsukada K *et al* 2017 *Phys. Rev. Lett.* **118** 262501
[20] Simon H 2007 *Nucl. Phys.* A **787** 102
[21] Antonov A N *et al* 2011 *Nucl. Instrum. Methods Phys. Res.* A **637** 60
[22] Ohnishi T *et al* 2015 *Phys. Scr.* **T166** 014071
[23] Baker A 1964 *Phys. Rev.* **134** B240
[24] Yennie D R, Boos F L and Ravenhall D G 1965 *Phys. Rev.* **137** B882
[25] Jakubassa-Amundsen D H 2014 *J. Phys. G: Nucl. Part. Phys.* **41** 075103
[26] Zhang C, Liu J and Ren Z 2016 *J. Phys. G: Nucl. Part. Phys.* **43** 045103
[27] Antonov A N *et al* 2005 *Phys. Rev.* C **72** 044307
[28] Karataglidis S and Amos K 2007 *Phys. Lett.* B **650** 148
[29] Roca-Maza X, Centelles M, Salvat F and Viñas X 2008 *Phys. Rev.* C **78** 044332
[30] Roca-Maza X, Centelles M, Salvat F and Viñas X 2013 *Phys. Rev.* C **87** 014304
[31] Jassim K S, Al-Sammarrae A A, Sharrad F I and Kassim H A 2014 *Phys. Rev.* C **89** 014304
[32] Yao J M, Bender M and Heenen P H 2015 *Phys. Rev.* C **91** 024301
[33] Marević P *et al* 2019 *Phys. Rev.* C **99** 034317
[34] Bertulani C A 2007 *J. Phys. G: Nucl. Part. Phys.* **34** 315
[35] Meucci A *et al* 2013 *Phys. Rev.* C **87** 054620
[36] Meucci A *et al* 2014 *Phys. Rev.* C **89** 034604
[37] Möller P, Nix J R, Myers W D and Swiatecki W J 1995 *At. Data Nucl. Data tables* **59** 185
[38] Raman S, Nestor C W and Tikkanen P 2001 *At. Data Nucl. Data tables* **78** 1
[39] Stone N J 2005 *At. Data Nucl. Data tables* **90** 75
[40] Scamps G, Lacroix D, Adamian G G and Antonenko N V 2013 *Phys. Rev.* C **88** 064327
[41] Moya de Guerra E 1980 *Ann. Phys.* **128** 286
[42] Moya de Guerra E 1986 *Phys. Rep.* **138** 293
[43] Liang T *et al* 2018 *Phys. Rev.* C **98** 044310
[44] Liu J *et al* 2019 *J. Phys. G: Nucl. Part. Phys.* **46** 055105
[45] Erler J *et al* 2012 *Nature* **486** 509
[46] Zhang Y, Matsuo M and Meng J 2011 *Phys. Rev.* C **83** 054301
[47] Pei J C, Kruppa A T and Nazarewicz W 2011 *Phys. Rev.* C **84** 024311
[48] Shi Y *et al* 2014 *Phys. Rev.* C **90** 014308
[49] Bhagwat A *et al* 2010 *Phys. Rev.* C **81** 044321
[50] Sarriguren P *et al* 2019 *Phys. Rev.* C **99** 034325
[51] Stoitsov M V *et al* 2007 *Phys. Rev.* C **76** 014308
[52] Vautherin D 1973 *Phys. Rev.* C **7** 296
[53] Zhou X, Hiyama E and Sagawa H 2016 *Phys. Rev.* C **94** 024331
[54] Greiner W and Reinhardt J 1992 *Quantum Electrodynamics* (Berlin: Springer)
[55] Moya de Guerra E *et al* 1991 *Nucl. Phys.* A **529** 68
[56] Horowitz C J 2014 *Phys. Rev.* C **89** 045503
[57] Pritychenko B, Birch M, Singh B and Horoi M 2016 *At. Data Nucl. Data tables* **107** 1
[58] Wang M *et al* 2017 *Chin. Phys.* C **41** 030003
[59] Sinha B B P *et al* 1973 *Phys. Rev.* C **7** 1930
[60] Frois B *et al* 1977 *Phys. Rev. Lett.* **38** 152

[61] Lightbody J W *et al* 1983 *Phys. Rev.* C **27** 113
[62] Cheal B and Flanagan K T 2010 *J. Phys. G: Nucl. Part. Phys.* **37** 113101
[63] Mondal C *et al* 2016 *Phys. Rev.* C **93** 064303
[64] Roca-Maza X, Colò G and Sagawa H 2018 *Phys. Rev. Lett.* **120** 202501
[65] Liu J, Ren Z and Xu C 2018 *J. Phys. G: Nucl. Part. Phys.* **45** 075103